

# Frequency-Aware Masked Autoencoders for Human Activity Recognition using Accelerometers

Niels R. Lorenzen<sup>1,2,3</sup>, Poul J. Jennum<sup>2</sup>, Emmanuel Mignot<sup>3</sup>, Andreas Brink-Kjaer<sup>1</sup>

**Abstract**— Wearable accelerometers are widely used for continuous monitoring of physical activity. Supervised machine learning and deep learning algorithms have long been used to extract meaningful activity information from raw accelerometry data, but progress has been hampered by the limited amount of labeled data that is publicly available. Exploiting large unlabeled datasets using self-supervised pretraining is a relatively new and underexplored approach in the field of human activity recognition (HAR).

We used a time-series transformer masked autoencoder (MAE) approach to self-supervised pretraining and propose a novel spectrogram-based loss function named the log-scale mean magnitude (LMM) loss. We compared MAE models pretrained with LMM to one trained with the mean squared error (MSE) loss. We leveraged the large unlabeled UK Biobank accelerometry dataset ( $n = 109k$ ) for pretraining and evaluated downstream HAR performance using linear classifier in a smaller labelled dataset.

We found that pretraining with the LMM loss improved performance compared to a model pretrained with the MSE loss, with balanced accuracies of 0.848 and 0.709, respectively. Further analysis revealed that better convergence of the LMM loss, but not the MSE loss significantly correlated with improved downstream performance ( $r=-0.61$ ,  $p=0.04$ ) for balanced accuracy). Finally, we compared our MAE models to the state-of-the-art for HAR, which was also pretrained on the UK Biobank accelerometry data using a different self-supervised learning approach. Our LMM-pretrained models performed better when fine-tuned using a linear classifier and performed comparably when fine-tuned using an LSTM classifier, while MSE-pretrained models consistently underperformed.

Our findings demonstrate that the LMM loss is a robust and effective method for pretraining MAE models on accelerometer data for HAR. Future work should explore optimizing loss function combinations and extending our approach to other tasks.

**Clinical Relevance**— Improved algorithms for human activity recognition, enables more accurate monitoring of physical activity, which is crucial for assessing mobility, rehabilitation progress, and chronic disease management.

## I. INTRODUCTION

Wearable accelerometry is a cost-effective tool for out-of-clinic health monitoring, with applications in human activity recognition (HAR) [1], [2], [3], [4], gait estimation [5], [6], and sleep monitoring [7]. The usefulness of these devices in understanding associations between different activities and

health relies heavily upon the quality of algorithms to detect such activities based on the data.

Until recently, supervised classical machine learning and deep learning has been state-of-the-art for HAR using wearable accelerometers [8], [9], [10], [11], [12]. However, since the arrival of foundation models for images and time-series relying on self-supervised pretraining [13], [14], multiple studies have employed different methods of self-supervised learning to wearable accelerometry data [2], [15], [16], [1], [4], [5]. However, only a few have done so with a large-scale dataset using the UK Biobank cohort [1], [5]. These both used multi-task learning based on a head-to-head comparison of masked reconstruction, multitask, and contrastive learning with a small amount of pretraining data [3]. However, the implementation of the masked autoencoder (MAE) in [2], [3] leaned heavily on the original implementation of the BERT language model [17] and misses possible improvements from more recent advances in MAEs for timeseries such as higher masking rates, patching, and rotational positional embeddings [14], [18], [19]. Furthermore, using frequency-domain information has proven useful for supervised HAR models [8], [9], [11]. Other work has shown that integrating frequency awareness in masked-autoencoders for other bio-signals led to better and more generalizable representations [20].

In this work, we introduce frequency awareness to a time-domain MAE by adapting a spectrogram loss developed for audio signals [21]. We explore how variations to this spectrogram loss affect convergence and fine-tuning performance in HAR. We show that a modern transformer MAE trained with this loss can perform on par with or better than the current state-of-the-art in HAR when pretrained using the large UK biobank cohort.

## II. METHODS

### A. Datasets

The unlabeled high-resolution wrist-worn accelerometer dataset from the UK Biobank [22] was used for self-supervised pretraining in this work. The dataset consists of 115,390 recordings of  $\sim 7$  days of free-living wrist-worn accelerometry from 103,618 participants. The data was recorded with 100 Hz sampling rate on Axivity AX3 devices. The sequence-aware nature of our transformer-based model calls for evaluation using labeled continuous recordings of free-living data rather than short scripted sequences of single behaviors as we expect the model to learn natural transitions between behaviors. This severely limits the amount of publicly available datasets for

[1] Department of Health Technology, Technical University of Denmark, Lyngby, Denmark.

[2] Danish Centre for Sleep Medicine, Copenhagen University Hospital-Rigshospitalet, Glostrup, Denmark.

[3] Department of Psychiatry and Behavioral Sciences, Stanford University, CA, USA.

downstream performance evaluation. For this purpose, we used the Capture-24 cohort [23] consisting of 151 participants with ~24 hours of data sampled at 100 Hz from Axivity AX3 devices. The data in this cohort has annotated day-time activities based on body-cam recordings and sleep periods based on a sleep-diary. The labels are reduced to the six categories bicycling, walking, mixed, vehicle, sit-stand, and sleep following previous research [1], [11].

### B. Preprocessing

Preprocessing included applying a 15Hz low-pass filter and resampling to 30Hz. The accelerometry data was then calibrated using the algorithm described in [24] without temperature correction. Stationary periods were detected using a 10 second moving standard deviation threshold of 0.013 g. Stationary periods of more than 90 minutes were classified as non-wear and dropped. Contiguous wear segments of at least 24 hours for the UK Biobank data and 1 hour for Capture-24 were kept. We excluded recordings without at least one period of the minimum wear time or those where calibration failed. This left 108,933 recordings from the UK biobank for which we used a 90-10 train-validation split and 149 for Capture-24 for which we used an 80-20 train-validation split.

### C. Model Training and Architecture

Data loading during pretraining was performed by loading 24hrs contiguous wear accelerometry data from 8 recordings. These were split into 32 50-minute windows with 5 minutes of overlap for each subject for a total batch size of 256 windows. In this way, each epoch, the model sees a random 24hrs of data per recording. Pretraining was split across two Tesla V100 SXM2 with 16GB of memory each and took ~24hrs for 20 epochs. For pretraining we used a base learning rate of  $1^{-3}$  with one-epoch linear learning rate scaling for burn-in followed by cosine annealing with warm restarts every epoch. During finetuning, the full 24-hour recordings were loaded into memory and divided into 50-minute windows with 45 minutes of overlap. This served as a form of data augmentation with the limited scale of finetuning data. Finetuning was done using a flat learning rate of  $1^{-3}$  on a single Tesla V100 SXM2 with 16GB of memory and took ~80min for 70 epochs. The architecture (Fig. 1a) is an encoder-only transformer with rotational embeddings (RoFormer) [19]. We trained models with 12 encoder blocks and an embedding dimension of 256. The feed-forward layers in the encoder blocks use SwiGLU activations [25] with a ratio of 8/3 hidden units to embedding dimensions. A residual connection with root-mean-square normalization is applied before each attention and feed-forward layer. The models have a total of ~10M parameters. Each 50-minute input signal was first segmented along the time dimension into 300 non-overlapping 10s patches and flattened along the channel dimension before being passed through a linear embedding layer, projecting the signal to a 256-dimensional embedding vector. During pretraining, a random 60% of the embeddings are replaced with a mask token, which is a learnable parameter vector. The embeddings are passed through the transformer encoder blocks where rotational embeddings [19] and self-attention are applied [26]. A linear layer acts as a reconstruction head, projecting the output feature vectors back into signal space. The reconstruction loss was calculated between the input and the reconstruction of the masked patches. During finetuning, no

masking was applied to the vector sequence, and the reconstruction head was replaced with a linear classification head. Only the classification head was optimized during finetuning.

### D. Loss Functions

For self-supervised pretraining we explored three different loss components, including mean squared error (MSE) and two frequency-based loss components. The MSE loss is typically used for image and timeseries MAEs relying on signal reconstruction [2], [14]. The first frequency-based loss function was the log-scale mean magnitude (LMM) loss (Fig. 1b) based on a log-scale magnitude loss introduced for audio signals in [21], with the change that we average the spectrogram in the time dimension for each 10-second patch. For the 3-axis accelerometry signals the STFT was applied axis-wise on the inputs and the reconstructions as

$$U(x) = \log(\min(\text{mean}_{\text{time}}(|\text{STFT}(x)|), \epsilon)), \quad (1)$$

where  $\epsilon = 10^{-1}$ . For a single input patch  $i$  from axis  $j$   $x_{ij}$  and corresponding reconstruction  $\hat{x}_{ij}$ , the LMM loss is computed as

$$\text{LMM}(x_{ij}, \hat{x}_{ij}) = \text{MSE}(U(x_{ij}), U(\hat{x}_{ij})) \quad (2)$$

Each patch was zero-padded on both sides so that the  $m^{\text{th}}$  FFT window was centered on the  $m \times H^{\text{th}}$  sample where  $H$  is the hop size of the FFT window. The Hann-window function was applied to each window before the FFT to mitigate edge effects. We tested the LMM loss in combination with the MSE loss since we discarded any intra-patch temporal information in averaging the magnitude of the STFT windows and not using phase information. The combined loss is defined as

$$\mathcal{L}_1(x_{ij}, \hat{x}_{ij}) = w_{\text{LMM}}\text{LMM}(x_{ij}, \hat{x}_{ij}) + w_{\text{MSE}}\text{MSE}(x_{ij}, \hat{x}_{ij}) \quad (3)$$

We also considered a loss on the time-variance of the spectral magnitudes as a way of introducing intra-patch temporal awareness without exact phase information. We denote this as the log-scale magnitude variance (LMV) loss, which was computed as

$$V(x) = \log(\min(\text{var}_{\text{time}}(|\text{STFT}(x)|), \epsilon)), \quad (4)$$

$$\text{LMV}(x_{ij}, \hat{x}_{ij}) = \text{MSE}(V(x_{ij}), V(\hat{x}_{ij})). \quad (5)$$

We test this in combination with the LMM loss:

$$\mathcal{L}_2(x_{ij}, \hat{x}_{ij}) = w_{\text{LMM}}\text{LMM}(x_{ij}, \hat{x}_{ij}) + w_{\text{LMV}}\text{LMV}(x_{ij}, \hat{x}_{ij}), \quad (6)$$

The reconstruction losses are only applied to masked input patches. Thus, for all 3 axes  $A$  full input signal  $X$  and its reconstruction  $\hat{X}$  divided into  $L$  patches:

$$\mathcal{L}(X, \hat{X}) = \frac{1}{\sum_{i=0}^{L-1} M_i} \sum_{i=0}^{L-1} M_i \sum_{j=0}^{A-1} \mathcal{L}(x_{ij}, \hat{x}_{ij}), \quad (7)$$

where  $M$  is a binary vector of length  $L$  with  $M_i = 1$  indicating that the  $i^{\text{th}}$  input patch was masked.

Finetuning for classifying human activities was done using the weighted cross entropy loss. Which for a single patch was computed as

$$\mathcal{L}_{\text{CE}}(y, \hat{y}) = - \sum_{i=0}^{C-1} w_i y_i \log \left( \frac{\exp(\hat{y}_i)}{\sum_{c=0}^{C-1} \exp(\hat{y}_c)} \right) \mathbf{1}(i \neq g), \quad (8)$$

where  $y$ ,  $\hat{y}$ , and  $w$  are vectors of length  $C$ ,  $C$  being the number of classes,  $y$  is binary vector with  $y_i = 1$  when  $i$  is the

index of the observed class and zero otherwise,  $\hat{y}$  contains the output logits of each class, and  $w$  is a vector of weights for each class corresponding to the inverse of class prevalence,  $g$  is the class index corresponding to a missing label, and  $\mathbf{1}(x)$  is the indicator function.

### E. Evaluation Metrics

We used balanced accuracy (BA) and Cohen’s kappa ( $\kappa$ ) to evaluate downstream classification performance. These were chosen as complimentary measures. BA has the property of reducing to  $\frac{1}{n_{classes}}$  if the classifier relies on the majority label, whereas  $\kappa$  does not account for label imbalance but measures overall agreement.

## III. EXPERIMENTS AND RESULTS

Models were pretrained on the full UK Biobank training partition for 20 epochs and performance was evaluated after 70 epochs of finetuning on the Capture-24 dataset for classification of bicycling, walking, mixed, vehicle, sit-stand, and sleep, unless otherwise specified. All reported loss values and metrics are for the validation sets.

### A. Loss Function Ablations

In the first experiments, we tested a model pretrained with the first combined loss (3). We vary the number of samples ( $N_{FFT}$ ) in the STFT windows effectively increasing the frequency resolution at higher values of  $N_{FFT}$  while reducing the number of windows in each signal patch since the hop length stays fixed at  $\frac{N_{FFT}}{2}$ . We varied  $N_{FFT}$  between 16, 32, 64, and 128 samples (Table 1) corresponding to  $\sim 0.5, 1, 2,$  and 4 seconds respectively. First, the MSE and LMM losses were investigated separately. The best performance for the LMM loss was observed with 64 samples  $N_{FFT}$  and 32 samples as a close second. The 16-sample window performed worst of the

TABLE I. FFT WINDOW SIZE TESTS

$w_{LMM}$	$w_{MSE}$	$N_{FFT}$	Balanced Accuracy	Cohen’s $\kappa$
0	1	-	0.709	0.649
1	0	16	0.779	0.721
		32	0.848	0.797
		64	<b>0.852</b>	<b>0.807</b>
		128	0.827	0.790
	0.1	16	0.813	0.741
		32	<b>0.851</b>	<b>0.806</b>
		64	0.840	0.796
		128	0.839	0.788

window sizes. However, the LMM loss outperformed the MSE loss at all values of  $N_{FFT}$  with increases of 0.07 - 0.143 in BA and 0.072 - 0.158 in  $\kappa$ . We then investigated the combined loss (3) with  $w_{MSE} = 0.1$  and  $w_{LMM} = 1$  to check for possible interactions with the MSE component and  $N_{FFT}$ . We found that this increased performance for most values of  $N_{FFT}$  except the 64-sample window. The biggest performance increase was seen for the 16-sample window. We chose a 32-sample STFT window for the following experiments due to similar performance with 64 samples with the added benefit of higher computational efficiency with shorter window lengths.

Next, we tested the second combined loss (6), varying the weight on the magnitude variance loss  $w_{LMV}$  while keeping  $w_{LMM} = 1$  (Table 2). We found no increase in performance with  $w_{LMV} > 0$  and did not include it in further experiments.

TABLE II. LMV LOSS TESTS

$w_{LMM}$	$w_{LMV}$	Balanced Accuracy	Cohen’s $\kappa$
1	0	<b>0.848</b>	<b>0.797</b>
	0.01	0.736	0.657
	0.1	0.824	0.766
	1	0.818	0.761

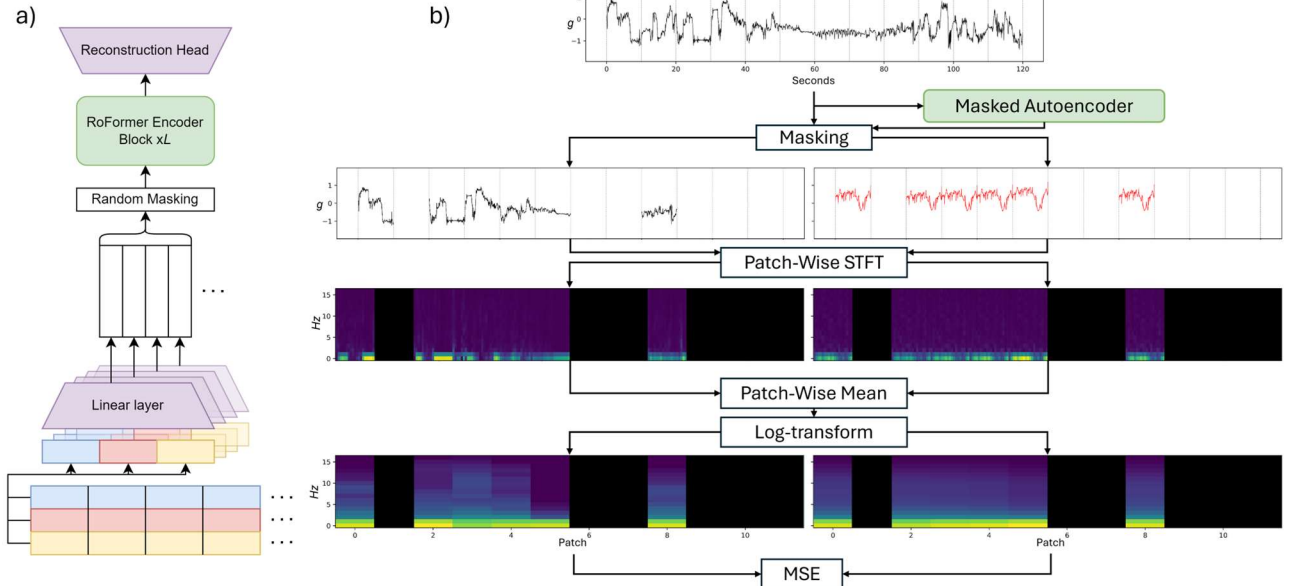


Figure 1. a) Architecture of the transformer masked autoencoder (MAE) during pretraining ( $L=12$ ). During finetuning the masking block is removed, and the reconstruction head replaced with a classification head. b) Illustration of the log-scale mean magnitude (LMM) loss for a single axis of the tri-axial input. First, the patched input (top, horizontal lines denote 10s patches) is passed through the MAE. Then masking is applied to the input and output reconstructions, only keeping the patches that were masked in the MAE. Next, magnitude spectrograms for each patch are computed, discarding phases, followed by temporal averaging and log-transformation. Finally, the MSE loss is calculated between these patch-wise log-scale mean spectrograms.

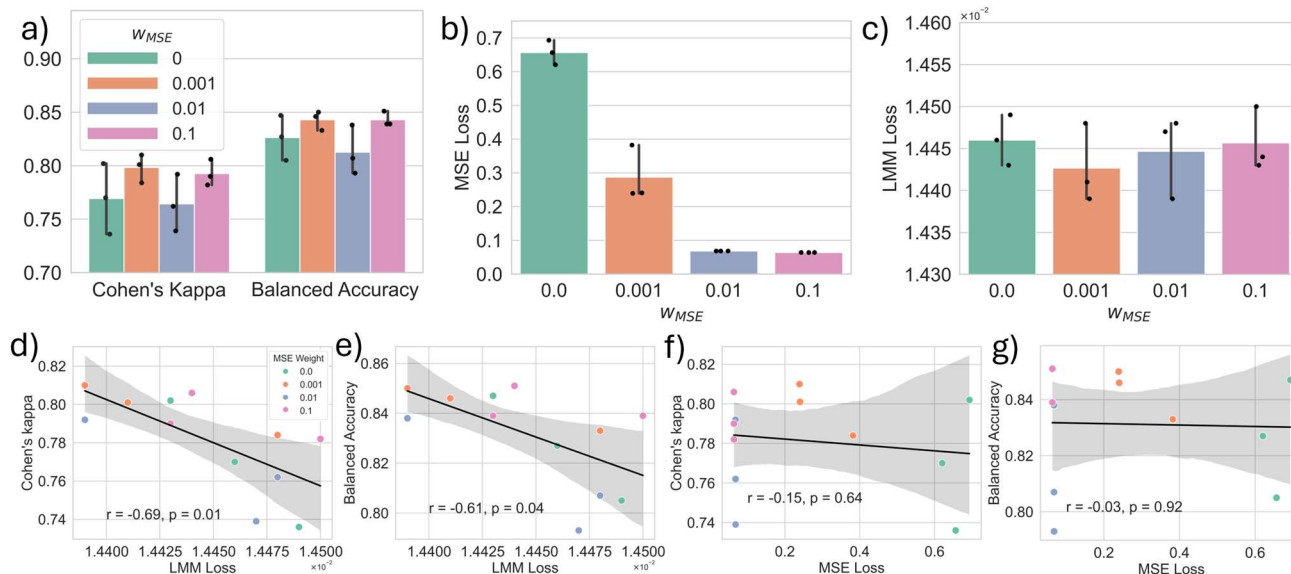


Figure 2. a-c) Effect of different values of  $w_{MSE}$  on a) finetuning HAR performance, b) pretraining MSE loss, and c) pretraining LMM loss, error bars  $\pm 95\%$  CI. d, e) Association between pretraining LMM loss and finetuning HAR performance for d) Cohen's kappa, pearson's  $r = -0.69$ ,  $p = 0.01$ , and e) balanced accuracy, pearson's  $r = -0.61$ ,  $p = 0.04$ . f, g) Association between pretraining MSE loss and finetuning HAR performance for f) Cohen's kappa, pearson's  $r = -0.15$ ,  $p = 0.64$ , and g) balanced accuracy, pearson's  $r = -0.03$ ,  $p = 0.92$ .

### B. Pretraining Convergence

Next, we assessed the convergence stability of the combined pretraining loss and the effect of pretraining convergence on downstream HAR performance. We used  $w_{MSE}$  values of 0, 0.001, 0.01, and 0.1 while keeping  $w_{LMM} = 1$ . We repeated the pretraining with three different random seeds for each value of  $w_{MSE}$ . First, we evaluated group differences in downstream performance (Fig. 2a). We did not observe any statistically significant difference in classification performance between any pairs of  $w_{MSE}$  for either BA or  $\kappa$ . We then explored the effect of  $w_{MSE}$  on the convergence of the MSE loss and the LMM loss components. We report the unweighted values of the MSE loss for comparability, including when  $w_{MSE} = 0$ . Unsurprisingly, increasing the value of  $w_{MSE}$  lead to significantly lower values of the MSE loss (Fig. 2b) with the two highest weights 0.01 and 0.1 leading to very stable convergence values. However, no significant effect was observed for  $w_{MSE}$  on the value of the LMM loss (Fig. 2c) and a similar spread was observed for all values of  $w_{MSE}$ . We examined linear associations between pretraining loss components and downstream classification performance (Fig 3). We found that decreasing values of the LMM loss was significantly associated with higher downstream performance for both  $\kappa$  ( $r = -0.69$ ,  $p = 0.01$ ) and BA ( $r = -0.61$ ,  $p = 0.04$ ) (Fig 3a, 3b). However, we did not find any significant association between the MSE loss and either  $\kappa$  ( $r = -0.15$ ,  $p = 0.64$ ) or BA ( $r = -0.03$ ,  $p = 0.92$ ) (Fig 3b, 3c). Although, we did observe that some of the best performing models were trained with  $w_{MSE}$  of 0.001 or 0.1 (Fig 2a). While this might be due to instability in the pretraining convergence we included models pretrained with  $w_{LMM}$  of 1 and  $w_{MSE}$  of 0 or 0.001 in the following experiments, referred to as  $MAE_{LMM}$  and  $MAE_{LMM+MSE}$ , respectively, moving forward for simpler notation.

### C. Masking Rate

In these experiments we did a small grid search for the masking rate used during pretraining with values of 0.3, 0.6, 0.75 and 0.9. We tested both  $MAE_{LMM}$  and  $MAE_{LMM+MSE}$ . We found that for both with and without the MSE component the best performance was achieved with a masking rate of 0.6 (Table 3).

### D. Data Volume Dependency

We assessed the sensitivity of the models on the amount of unlabeled data seen during pretraining by varying the percentage of the total UK biobank training set used between 20, 40, 60, 80, and 100 percent. For the reduced amounts of training data, the number of pretraining epochs was increased to keep the total number of training steps constant. The reduced training sets are subsets of all the larger sets and the validation set remained the same. This was done with  $w_{MSE}$  values of 0 and 0.001. For both values of  $w_{MSE}$  we observed that the best performance was achieved with 100 percent of the training data (Table 4). However, we did not see a steady performance decrease as we reduce the amount of pretraining data. We observed a drastic performance drop when using 40 percent of the pretraining data compared to both 60 and 20 percent for both values of  $w_{mse}$ . We also note that we did not

TABLE III. MASKING RATES

Model type	Masking rate	Balanced Accuracy	Cohen's Kappa
$MAE_{LMM}$	0.3	0.839	0.783
	0.6	<b>0.848</b>	<b>0.797</b>
	0.75	0.762	0.666
	0.9	0.627	0.501
$MAE_{LMM+MSE}$	0.3	0.815	0.755
	0.6	<b>0.850</b>	<b>0.804</b>
	0.75	0.595	0.457
	0.9	0.803	0.749

TABLE IV. VARYING AMOUNT OF PRETRAINING DATA

Model type	Pretrain percent	Balanced Accuracy	Cohen's Kappa
MAE <sub>LMM</sub>	20	0.705	0.602
	40	0.547	0.395
	60	0.720	0.628
	80	0.763	0.691
	100	0.848	0.797
MAE <sub>LMM+MSE</sub>	20	0.580	0.461
	40	0.545	0.390
	60	0.774	0.719
	80	0.764	0.704
	100	0.850	0.804

observe a performance plateau suggesting that we might see a performance increase with even more pretraining data. Next, we evaluated the sensitivity of the models pretrained on the full pretraining sample to the amount of finetuning data. The total number of training steps were kept constant by

increasing the number of epochs. Both models achieved the best performance when finetuned on all the training data (Table 5). However, they also displayed robustness even when only using 5 percent of the finetuning data corresponding to 5 participants with a performance difference of only 0.04 and 0.033 in BA for MAE<sub>LMM</sub> and MAE<sub>LMM+MSE</sub>, respectively,

compared to the full finetuning set. The increased performance at 10 and 5 percent compared to 20 percent of the finetuning data might be explained by the weighting of the classes in the CE loss (8) changing with the prevalence of individual labels in the subsets. This could in principle lead to more optimal class weights for the validation set.

E. Representations and Performance

We used UMAP and PCA to visualize the representations learned by our MAE<sub>LMM</sub> and MAE<sub>LMM+MSE</sub> models, as well as one trained with only the MSE loss (MAE<sub>MSE</sub>) and compared them to their confusion matrices (Fig. 3). The pretrained encoders were used to generate non-overlapping embeddings of the Capture-24 data. In the UMAP projections of MAE<sub>LMM</sub> (Fig. 3a) we saw good separation between most classes except ‘mixed’, ‘walking’, and a subset of ‘sit-stand’. This overlap was partially expected as the ‘mixed’ class includes activities that involve walking. The ‘bicycling’ class was strongly separated from the rest. These observations align well with the confusion matrix (Fig. 3g), where we see most confusion between ‘walking’, ‘mixed’ and ‘sit-stand’ to a lesser degree, while ‘bicycling’ and ‘sleep’ are almost perfectly classified. For most of the classes we also observed some intra-class

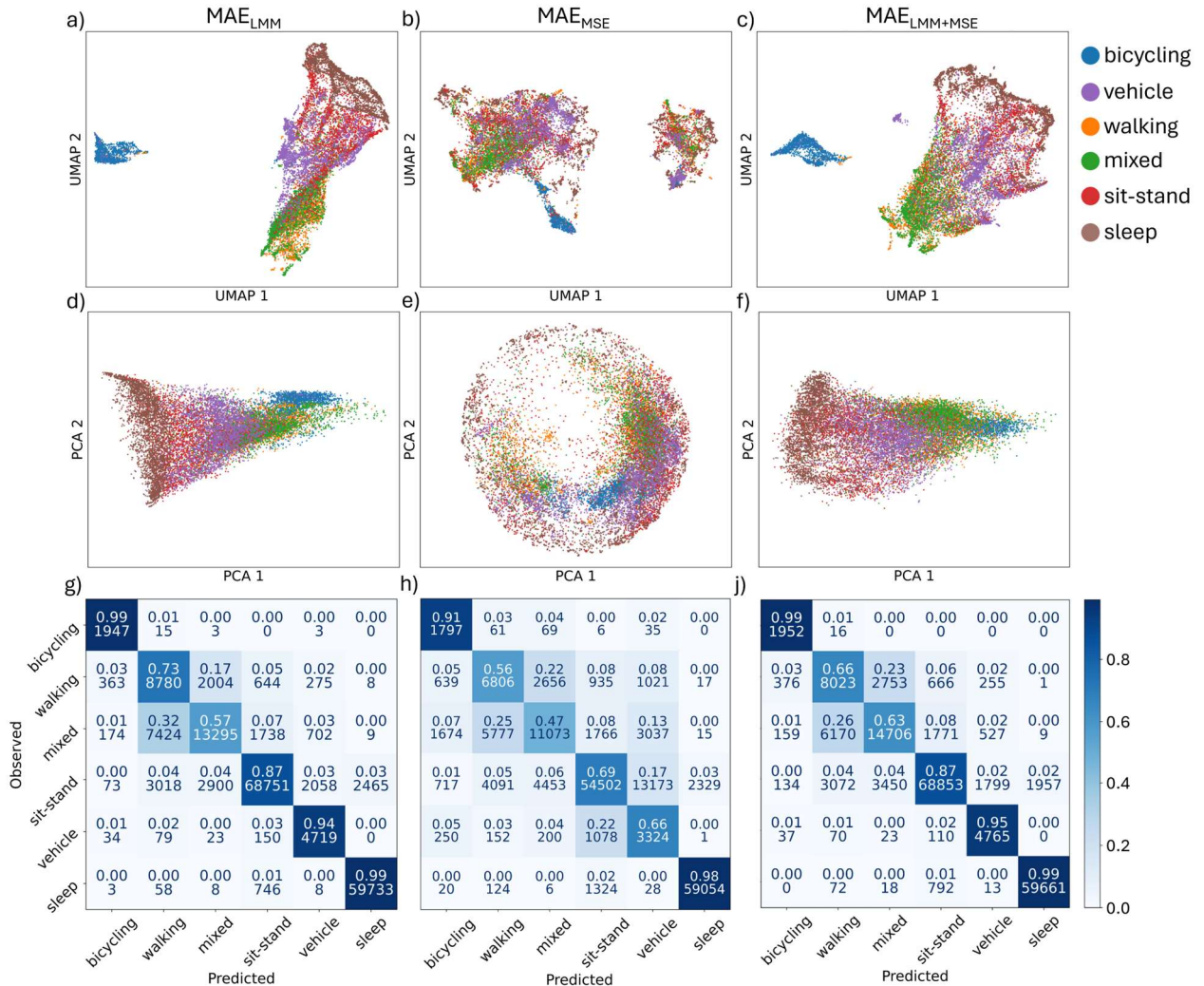


Figure 3. a-c) UMAP projections of embeddings from a) MAE<sub>LMM</sub>, b) MAE<sub>MSE</sub>, and c) MAE<sub>LMM+MSE</sub>. d-f) PCA projections of embedding from d) MAE<sub>LMM</sub>, e) MAE<sub>MSE</sub>, and f) MAE<sub>LMM+MSE</sub>. g-j) Confusion matrices for g) MAE<sub>LMM</sub>, h) MAE<sub>MSE</sub>, and j) MAE<sub>LMM+MSE</sub>.

TABLE V. VARYING AMOUNT OF FINETUNING DATA

Model Type	Finetune Percent	Balanced Accuracy	Cohen's Kappa
MAE <sub>LMM</sub>	5	0.808	0.779
	10	0.812	0.797
	20	0.795	0.772
	40	0.838	0.795
	60	0.844	0.792
	80	0.845	0.796
	100	0.848	0.797
MAE <sub>LMM+MSE</sub>	5	0.817	0.793
	10	0.818	0.801
	20	0.812	0.785
	40	0.839	0.801
	60	0.843	0.797
	80	0.847	0.805
	100	0.850	0.804

structures, which suggest that more fine-grained labels could be resolved. In the corresponding PCA (Fig. 3d) we found that the first PC corresponded to increasing intensity of the activities while the second PC showed no clear pattern with these labels except for separation of ‘walking’ and ‘bicycling’. For the MAE<sub>MSE</sub> embeddings (Fig. 3b, 3e) we generally observed much weaker clustering of the classes with two distinct clusters appearing in the UMAP plot which both seemed to contain most classes except for ‘bicycling’ which was still nicely clustered. The PCA revealed a circular arrangement with ‘sleep’ embeddings along the periphery and higher intensity classes towards the center. The confusion matrix (Fig. 3h) revealed more confusion between ‘sit-stand’ and ‘vehicle’ but surprisingly strong performance for ‘sleep’ despite no strong clustering of the class in the embedding space. The combined MAE<sub>LMM+MSE</sub> model (Fig. 3c, 3f) showed very similar embedding patterns to MAE<sub>LMM</sub> (Fig. 3a, 3d) with slightly less sharply delineated clusters. However, this did not impair performance for any specific class (Fig. 3j).

#### F. Benchmarking

Here we benchmark our MAE models against HARNet10, the current state-of-the-art [1] in HAR from wrist-worn accelerometer data. We finetuned our models with either a linear layer or 2 long-short-term memory (LSTM) layers and a linear layer. We included the LSTM finetuning with 50 minutes of input data since our transformer-based models are inherently sequence-aware with 50 minutes of input while the ResNet-based HARNet10 takes in only one 10-second segment at a time. For HARNet10 we used a multi-layer perceptron (MLP) instead of a linear layer as was done in [1]. When finetuning just a linear layer our MAE<sub>LMM</sub> (BA 0.848) and MAE<sub>LMM+MSE</sub> (BA 0.850), outperformed HARNet10 with just a MLP (BA 0.748) (Table 6). However, when finetuning with LSTM layers the performances were near identical for MAE<sub>LMM</sub> (BA 0.869), MAE<sub>LMM+MSE</sub> (BA 0.867), and HARNet10 (BA 0.866). Finetuning with LSTM layers led to overfitting after  $\sim 2$  epochs for all models so we report the results for the epoch where validation BA peaked. The MAE<sub>MSE</sub> model performed worst of the pretrained model with both linear (BA 0.709) and LSTM (BA 0.810) finetuning. We also trained a full transformer model, identical in architecture to our MAE models, from scratch for comparison and found that it performed worst overall (BA 0.593).

TABLE VI. BENCHMARKING

Model	Finetuning Method	Balanced Accuracy	Cohen's Kappa
MAE <sub>LMM</sub>	Linear	0.848	0.802
	LSTM	<b>0.869</b>	<b>0.832</b>
MAE <sub>MSE</sub>	Linear	0.709	0.649
	LSTM	0.810	0.753
MAE <sub>LMM+MSE</sub>	Linear	<b>0.850</b>	<b>0.804</b>
	LSTM	0.867	0.831
Transformer <sub>scratch</sub>	-	0.593	0.682
HARNet10	MLP	0.748	0.671
	LSTM	0.866	0.825

#### IV. DISCUSSION

In this work, we demonstrated that a transformer MAE can achieve state-of-the-art performance for HAR when pretrained using the LMM loss, highlighting the potential of pretraining sequence-based models for free-living HAR. However, it also showed that sequence modelling is not enough to make up for bad representations obtained using the MSE loss. We showed the importance of testing the uncertainty of pretraining convergence when characterizing a self-supervised learning method, something that is often neglected in current literature, likely due to the high demand on GPU capacity. We found a strong association between the convergence of the LMM loss component and downstream performance. This suggests stabilizing and improving this convergence as a promising avenue for future research. In this work we did not find any solid evidence that including any intra-patch temporal information through the MSE or LMV losses contributed to learning useful representations for downstream HAR. It seems likely that reconstructing the signal sample for sample in relatively large patches as enforced by the time-domain MSE loss is simply too difficult a task for effective learning. This likely also explains the deterioration in performance observed at the highest frequency resolution we tested for the LMM loss which was our initial motivation for not simply using the full Fourier transform of each patch. Even so, more work is likely needed to fully characterize how the MSE and LMM loss components can complement each other due to instability in the pretraining convergence.

In our benchmarking experiments we found that our LMM trained MAE models outperformed HARNet10 when training a simple classifier, but it is unclear whether this is due to the quality of the learned representations or the sequence-aware nature of our model. We included the LSTM classifier to test this and found that it removed the performance gap. However, it is important to note that any advantage brought by sequence modelling in our MAE models can only be due to detection of natural state transitions in the data, since no sequence-aware training is done with labeled data, while the LSTM is allowed to learn sequential patterns in the labels. This possibly explains the overfitting we observed with the LSTM classifiers. Furthermore, the LSTM layers significantly increased GPU memory usage when finetuning HARNet10. This means that this method of finetuning has poor scalability to increasing sequence lengths. This showcases the advantages of performing sequence modelling during pretraining.

A key limitation of this work is the limited scope of the downstream task. Testing how this pretraining approach generalizes to free-living HAR in other cohorts and devices

will be key to demonstrate the strength of the approach and highlights the need for more such datasets to be collected and made available.

## V. CONCLUSION

We introduced masked reconstruction of frequency magnitudes with the LMM loss as a method for self-supervised pretraining for HAR using high-resolution wrist-worn accelerometry. We showed the strength of the approach compared to current state-of-the-art and compared to time-domain masked reconstruction. This is to our knowledge the first demonstration of the viability of pretraining transformer MAEs on large-scale high-resolution accelerometry data for HAR.

## REFERENCES

- [1] H. Yuan et al., “Self-supervised learning for human activity recognition using 700,000 person-days of wearable data,” *Npj Digit. Med.*, vol. 7, no. 1, pp. 1–10, Apr. 2024, doi: 10.1038/s41746-024-01062-3.
- [2] H. Haresamudram et al., “Masked reconstruction based self-supervision for human activity recognition,” in *Proceedings of the 2020 ACM International Symposium on Wearable Computers*, in ISWC '20. New York, NY, USA: Association for Computing Machinery, Sep. 2020, pp. 45–49. doi: 10.1145/3410531.3414306.
- [3] H. Haresamudram, I. Essa, and T. Plötz, “Assessing the State of Self-Supervised Human Activity Recognition using Wearables,” Nov. 19, 2022, arXiv: arXiv:2202.12938. Accessed: Jun. 12, 2024. [Online]. Available: <http://arxiv.org/abs/2202.12938>
- [4] A. Saeed, T. Ozcelebi, and J. Lukkien, “Multi-task Self-Supervised Learning for Human Activity Detection,” *Proc ACM Interact Mob Wearable Ubiquitous Technol*, vol. 3, no. 2, p. 61:1-61:30, Jun. 2019, doi: 10.1145/3328932.
- [5] Y. E. Brand et al., “Self-supervised learning of wrist-worn daily living accelerometer data improves the automated detection of gait in older adults,” *Sci. Rep.*, vol. 14, no. 1, p. 20854, Sep. 2024, doi: 10.1038/s41598-024-71491-3.
- [6] S. R. Small et al., “Development and Validation of a Machine Learning Wrist-worn Step Detection Algorithm with Deployment in the UK Biobank,” Feb. 22, 2023, medRxiv. doi: 10.1101/2023.02.20.23285750.
- [7] M. R. Patterson et al., “40 years of actigraphy in sleep medicine and current state of the art algorithms,” *Npj Digit. Med.*, vol. 6, no. 1, pp. 1–7, Mar. 2023, doi: 10.1038/s41746-023-00802-1.
- [8] K. Ellis, J. Kerr, S. Godbole, J. Staudenmayer, and G. Lanckriet, “Hip and Wrist Accelerometer Algorithms for Free-Living Behavior Classification,” *Med. Sci. Sports Exerc.*, vol. 48, no. 5, p. 933, May 2016, doi: 10.1249/MSS.0000000000000840.
- [9] A. Mannini, S. S. Intille, M. Rosenberger, A. M. Sabatini, and W. Haskell, “Activity Recognition Using a Single Accelerometer Placed at the Wrist or Ankle,” *Med. Sci. Sports Exerc.*, vol. 45, no. 11, p. 2193, Nov. 2013, doi: 10.1249/MSS.0b013e31829736d6.
- [10] S. Zhang, A. V. Rowlands, P. Murray, and T. L. Hurst, “Physical activity classification using the GENE wrist-worn accelerometer,” *Med. Sci. Sports Exerc.*, vol. 44, no. 4, pp. 742–748, Apr. 2012, doi: 10.1249/mss.0b013e31823bf95c.
- [11] M. Willetts, S. Hollowell, L. Aslett, C. Holmes, and A. Doherty, “Statistical machine learning of sleep and physical activity phenotypes from sensor data in 96,220 UK Biobank participants,” *Sci. Rep.*, vol. 8, no. 1, p. 7961, May 2018, doi: 10.1038/s41598-018-26174-1.
- [12] A. P. Creagh, F. Lipsmeier, M. Lindemann, and M. D. Vos, “Interpretable deep learning for the remote characterisation of ambulation in multiple sclerosis using smartphones,” *Sci. Rep.*, vol. 11, no. 1, p. 14301, Jul. 2021, doi: 10.1038/s41598-021-92776-x.
- [13] M. Cheng, Q. Liu, Z. Liu, H. Zhang, R. Zhang, and E. Chen, “TimeMAE: Self-Supervised Representations of Time Series with Decoupled Masked Autoencoders,” Mar. 13, 2023, arXiv: arXiv:2303.00320. Accessed: Jun. 12, 2024. [Online]. Available: <http://arxiv.org/abs/2303.00320>
- [14] K. He, X. Chen, S. Xie, Y. Li, P. Dollár, and R. Girshick, “Masked Autoencoders Are Scalable Vision Learners,” Dec. 19, 2021, arXiv: arXiv:2111.06377. doi: 10.48550/arXiv.2111.06377.
- [15] H. Haresamudram, I. Essa, and T. Plötz, “Contrastive Predictive Coding for Human Activity Recognition,” *Proc ACM Interact Mob Wearable Ubiquitous Technol*, vol. 5, no. 2, p. 65:1-65:26, Jun. 2021, doi: 10.1145/3463506.
- [16] K. Shah, D. Spathis, C. I. Tang, and C. Mascolo, “Evaluating Contrastive Learning on Wearable Timeseries for Downstream Clinical Outcomes,” Nov. 13, 2021, arXiv: arXiv:2111.07089. doi: 10.48550/arXiv.2111.07089.
- [17] J. Devlin, M.-W. Chang, K. Lee, and K. Toutanova, “BERT: Pre-training of Deep Bidirectional Transformers for Language Understanding,” May 24, 2019, arXiv: arXiv:1810.04805. doi: 10.48550/arXiv.1810.04805.
- [18] Y. Nie, N. H. Nguyen, P. Sinthong, and J. Kalagnanam, “A Time Series is Worth 64 Words: Long-term Forecasting with Transformers,” Mar. 05, 2023, arXiv: arXiv:2211.14730. doi: 10.48550/arXiv.2211.14730.
- [19] J. Su, Y. Lu, S. Pan, A. Murtagh, B. Wen, and Y. Liu, “RoFormer: Enhanced Transformer with Rotary Position Embedding,” Nov. 08, 2023, arXiv: arXiv:2104.09864. Accessed: Jun. 12, 2024. [Online]. Available: <http://arxiv.org/abs/2104.09864>
- [20] R. Liu et al., “Frequency-Aware Masked Autoencoders for Multimodal Pretraining on Biosignals,” Apr. 18, 2024, arXiv: arXiv:2309.05927. Accessed: Sep. 19, 2024. [Online]. Available: <http://arxiv.org/abs/2309.05927>
- [21] S. O. Arik, H. Jun, and G. Diamos, “Fast Spectrogram Inversion using Multi-head Convolutional Neural Networks,” *IEEE Signal Process. Lett.*, vol. 26, no. 1, pp. 94–98, Jan. 2019, doi: 10.1109/LSP.2018.2880284.
- [22] A. Doherty et al., “Large Scale Population Assessment of Physical Activity Using Wrist Worn Accelerometers: The UK Biobank Study,” *PLOS ONE*, vol. 12, no. 2, p. e0169649, Feb. 2017, doi: 10.1371/journal.pone.0169649.
- [23] S. Chan et al., “CAPTURE-24: A large dataset of wrist-worn activity tracker data collected in the wild for human activity recognition,” Feb. 29, 2024, arXiv: arXiv:2402.19229. Accessed: Jul. 11, 2024. [Online]. Available: <http://arxiv.org/abs/2402.19229>
- [24] V. T. van Hees et al., “Autocalibration of accelerometer data for free-living physical activity assessment using local gravity and temperature: an evaluation on four continents,” *J. Appl. Physiol.*, vol. 117, no. 7, pp. 738–744, Oct. 2014, doi: 10.1152/jappphysiol.00421.2014.
- [25] N. Shazeer, “GLU Variants Improve Transformer,” Feb. 12, 2020, arXiv: arXiv:2002.05202. doi: 10.48550/arXiv.2002.05202.
- [26] A. Vaswani et al., “Attention Is All You Need,” Aug. 02, 2023, arXiv: arXiv:1706.03762. doi: 10.48550/arXiv.1706.03762.